

Mesoporous bioactive glass as a multifunctional system for bone regeneration and controlled drug release

*Original*

Mesoporous bioactive glass as a multifunctional system for bone regeneration and controlled drug release / Baino, Francesco; Fiorilli, SONIA LUCIA; Mortera, RENATO SILVIO; Onida, Barbara; Saino, E.; Visai, L.; Verne', Enrica; VITALE BROVARONE, Chiara. - In: JOURNAL OF APPLIED BIOMATERIALS & FUNCTIONAL MATERIALS. - 10:(2012), pp. 12-21. [10.5301/JABFM.2012.9270]

*Availability:*

This version is available at: 11583/2429995 since:

*Publisher:*

Wichtig Editore

*Published*

DOI:10.5301/JABFM.2012.9270

*Terms of use:*

This article is made available under terms and conditions as specified in the corresponding bibliographic description in the repository

*Publisher copyright*

(Article begins on next page)

# Mesoporous bioactive glass as a multifunctional system for bone regeneration and controlled drug release

Francesco Baino<sup>1,\*</sup>, Sonia Fiorilli<sup>1</sup>, Renato Mortera<sup>1</sup>, Barbara Onida<sup>1</sup>, Enrica Saino<sup>2,3</sup>, Livia Visai<sup>2,3,4,5</sup>, Enrica Verné<sup>1</sup>, Chiara Vitale-Brovarone<sup>1</sup>

This is the author post-print version of an article published on *JOURNAL OF APPLIED BIOMATERIALS & FUNCTIONAL MATERIALS*, Vol. 10, pp. 12-21, 2012 (ISSN 2280-8000).

The final publication is available at

<http://www.jab-fm.com/article/mesoporous-bioactive-glass-as-a-multifunctional-system-for-bone-regeneration-and-controlled-drug-release>.

This version does not contain journal formatting and may contain minor changes with respect to the published edition.

The present version is accessible on PORTO, the Open Access Repository of the Politecnico of Torino, in compliance with the publisher's copyright policy.

Copyright owner: *Wichtig Editore*.

<sup>1</sup>Materials Science and Chemical Engineering Department, Politecnico di Torino, Corso Duca degli Abruzzi 24, 10129 Torino, Italy

<sup>2</sup>"A. Castellani" Biochemistry Department, Medicine Section, University of Pavia, Via Taramelli 3/b, 27100 Pavia, Italy

<sup>3</sup>Center for Tissue Engineering (CIT), University of Pavia, Via Ferrara 1, 27100 Pavia, Italy

<sup>4</sup>"S. Maugeri" Foundation, IRCCS, Via S. Maugeri 4, 27100 Pavia, Italy

<sup>5</sup>International Centre For Studies and Research In Biomedicine (ICB), L-2015 Luxembourg

\*Corresponding author: Francesco Baino

Tel.: +39 011 564 4668

Fax: +39 011 564 4699

E-mail: [francesco.baino@polito.it](mailto:francesco.baino@polito.it)

## ACKNOWLEDGEMENTS

The authors would like to acknowledge financial support by: (1) PRIN 2006-2008, financed by the “Ministero Italiano dell’Università e della Ricerca” (MIUR); (2) project “SAL-45” financed by Regione Lombardia; (3) project titled “Nanomedicine in ageing-associated prototypic diseases: activation of a scientific and technological platform challenging seminal aspects of pathogenesis, diagnosis and therapy” financed by Fondazione Alma Mater Ticinensis (2010). L.V. would like to acknowledge financial support by the International Centre For Studies And Research In Biomedicine (ICB), Luxembourg.

**Conflict of interest:** None.

**Key words:** Mesoporous glasses, Bioactivity, Biocompatibility, Drug release, Bone grafting, Tissue engineering.

## Abstract

*Purpose:* Coupling in a single device the potential for bone regeneration and the ability for *in situ* controlled drug release is a challenging field of research in bone tissue engineering; in an attempt to pursue this aim, membranes of mesoporous bioactive glass (MBG) belonging to the  $\text{SiO}_2\text{-P}_2\text{O}_5\text{-CaO}$  ternary system were produced and characterized.

*Materials and methods:* The glass was synthesized via a sol-gel route coupled with evaporation-induced self-assembly process by using a non-ionic block co-polymer as a mesostructure former. MBG structure and morphology, as well as mesopores size and shape, were investigated by X-ray diffraction, transmission electron microscopy and  $\text{N}_2$  adsorption-desorption measurements. *In vitro* bioactivity was investigated by soaking MBG membranes in simulated body fluid (SBF) for different time frames. Ibuprofen was encapsulated into MBG pores and the drug release kinetics in SBF were assessed. Biological tests by using SAOS-2 cells were performed to evaluate the material cytocompatibility.

*Results:* The material exhibited a high ability of inducing hydroxyapatite formation on its surface (bioactivity). Drug release kinetics in SBF are very similar to those obtained for mesoporous silica having mesopores size comparable to that of the prepared MBG (~5 nm). No evidence of cells viability depression was detected during *in vitro* culture, which demonstrates the good biological compatibility of the material.

*Conclusions:* The easiness of tailoring and shaping, the highly bioactive and biocompatible behaviour and the drug uptake/release ability of the prepared materials can suggest their use as “smart” multifunctional grafts for bone reconstructive surgery.

## INTRODUCTION

Mesostructured materials belong to the class of nanomaterials, whose properties can be tailored at the nanometrical scale. Specifically, according to IUPAC classification mesoporous solids are characterized by pores ranging within 2-50 nm (1). These materials are generally obtained by coupling a sol-gel method, that is very effective to prepare glasses and ceramics at room temperature, with a supramolecular self-assembling process (2). This particular approach is possible by taking advantage of hydrophobic/hydrophilic features of some molecules, *i.e.* surfactants, to prepare supramolecular aggregates, called micellae (3).

The first successful synthesis of ordered mesostructured silicas (OMSs) was reported in the early 1990s, when researchers of Mobil Oil Corporation used surfactants as structure-directing agents (SDAs) (4). Since then, a wide range of OMSs, such as the hexagonal phases MCM-41 and SBA-15, have been prepared and investigated (4,5).

The skill to tailor the channels size depending on the synthesis conditions, and the ordered pores structure of OMSs make these materials promising matrices for the encapsulation of functional molecules, such as dyes, drugs or enzymes. In particular, OMSs have attracted increasing interest in biomaterials science as devices for controlled drug release (6). For this purpose, recent studies have proposed composite hierarchical systems, coupling silica mesophases and bioactive scaffolds, in order to obtain multifunctional devices able to combine bone-bonding properties with drug delivery ability (7-10).

As regards the applications in bone tissue engineering, it should be taken into account that as-such OMSs are not very suitable as bone fillers due their lack of bioactivity, that nevertheless can be opportunely induced. In fact, MCM-41 exhibited a good bioactive behaviour when its walls were doped with phosphorus (11) or by adding small quantities of bioactive glasses (12). Composite systems formed by MCM-41 and bioactive glass-

ceramic scaffolds, necessary to guarantee implant bioactivity, have been also recently proposed for bone tissue engineering (7-10).

The materials traditionally used for bone replacement, e.g. natural or synthetic hydroxyapatite (HA) (13), calcium phosphates (14) and bioactive glasses and glass-ceramics (BGs and BGCs) (15,16), which have been widely investigated since the early 1970s, are able to chemically bond to living bone without the formation of scar or fibrous tissue around the implant owing to the growth of a bone-like apatite layer on their surface in the course of the so-called “bioactivity process” (17). In particular, BGs are glasses of complex composition containing modifier oxides, e.g. CaO, Na<sub>2</sub>O and K<sub>2</sub>O, that locally interrupt the SiO<sub>2</sub>-based network. The bioactivity process is due to ion-exchange phenomena between the glass, which usually releases alkaline ions (Ca<sup>2+</sup>, Na<sup>+</sup>, K<sup>+</sup>), and the solution or the biological fluids put into contact with the implant.

It is known that the formation of an apatite layer on sol-gel glasses surface is related both to the structure and to the composition of the material, whereas BGs obtained via traditional melting routes show a direct dependence only from the composition (18). In fact, it was demonstrated that an increase of the specific surface area and pores volume in sol-gel BGs highly accelerates the HA formation kinetics, thereby enhancing the bone-bonding ability of the material (19,20). Recently, ordered SiO<sub>2</sub>-based mesoporous bioactive glasses (MBGs) have been synthesized through a combination between supramolecular chemistry and sol-gel process (21-23). The potential carried by this new class of biomaterials is remarkable, and, for instance, the use of MBGs as drug release systems (21,22), bone fillers (23) and components of glass cements inducing accelerated *in vitro* apatite formation (24) have been proposed.

In the present work, a MBG belonging to the SiO<sub>2</sub>-P<sub>2</sub>O<sub>5</sub>-CaO ternary system has been synthesized in different forms (powders and membranes of adjustable thickness) and its features were investigated in detail by means of structural and morphological analysis, *in*

*vitro* bioactivity tests and biological compatibility assay. In addition, the drug uptake and release ability of the material was evaluated by using ibuprofen as a model drug. The great potential of the prepared MBG as a multifunctional material able to couple bone regeneration ability, in virtue of its excellent bioactivity, with drug release properties was particularly highlighted. In addition, the easiness and versatility of shaping the MBG in form of membranes could carry valuable advantages also from a surgical viewpoint, in an attempt to design and manufacture patient-designed bone grafts. In such a context, an ever better synergy between surgeons and materials scientists will be very desirable and appreciated.

## MATERIALS AND METHODS

### *Materials synthesis*

In this work, a glass with ordered mesostructure was produced by coupling a traditional sol-gel method with the evaporation-induced self-assembly (EISA) process (25), following the procedure previously reported by Yan *et al.* (26). An amphiphilic triblock copolymer with sequence poly(ethylene glycole)-poly(propylene glycole)-poly(ethylene glycole) (PEG-PPG-PEG), commercially called Pluronic 123 (P123), was used as a structure directing agent (SDA) (5). Briefly, 2.0 g of P123 ( $M_w = 5800$  Da; Aldrich) were dissolved in 60.0 g of ethanol (99.5%, Sigma-Aldrich) and 1.0 g of 0.5 M HCl. After continuous magnetic stirring ( $\sim 400$  rpm) at 35 °C for 1 h, till P123 is completely dissolved, the glass oxides precursors, *i.e.* 6.7 g of tetraethyl orthosilicate (TEOS; 98.0%, Sigma-Aldrich), 0.73 g of triethyl phosphate (TEP; 99.8%, Sigma-Aldrich) and 1.4 g of calcium nitrate,  $\text{Ca}(\text{NO}_3)_2 \cdot 4\text{H}_2\text{O}$  (Sigma-Aldrich) (molar ratio Si/Ca/P = 80:15:5), were added to the synthesis batch (pH < 1.0). The batch was continuously stirred at 35 °C for 24 h; then, the sol was cast into glass

moulds to undergo the EISA process at room temperature (RT). The gelation occurred after ~36 h; after 7 days of ageing, the dried gels were carefully removed from the moulds as transparent membranes and finally calcined at 700 °C in air for 5 h (heating rate and cooling rate set at 1 and 10 °C·min<sup>-1</sup> respectively). The steps involved in the preparation method of MBGs are resumed in Figure 1.

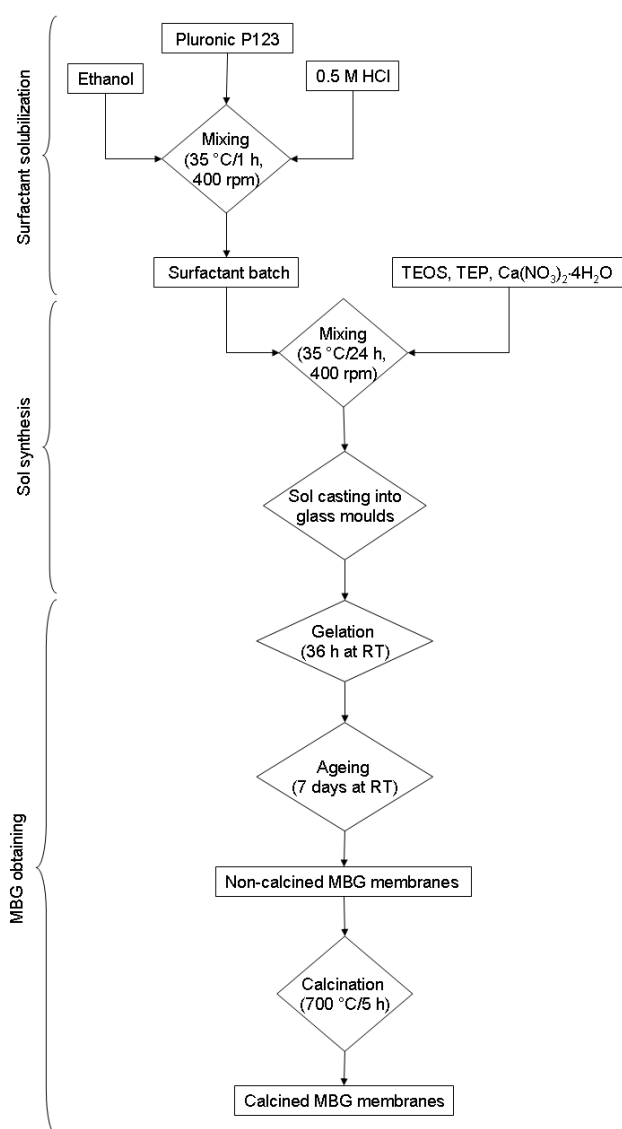


**Fig. 1 - Flow-chart of the procedure followed for manufacturing the mesoporous glass.**

### Materials characterization

The MBG was investigated by means of wide-angle ( $2\theta$  within  $10-70^\circ$ ) and low-angle ( $2\theta$  within  $0.8-4^\circ$ ) X-ray diffraction (XRD, X'Pert Philips diffractometer with Bragg-Brentano camera, Cu anode and  $K\alpha$  radiation); specifically, the latter one was necessary to assess the mesostructure symmetry.

Compositional investigations on the samples before and after calcination were carried out by energy dispersive spectroscopy (EDS; Philips Edax 9100); the samples were silver-coated before analysis.

Nitrogen ( $N_2$ ) adsorption-desorption porosimetry measurements at 77 K (Quantachrome Autosorb1) were carried out on the MBG ground in powders; in particular, the specific surface area (SSA) was assessed by using the Brunauer-Emmet-Teller (BET) method (27), whereas the pores size distribution was determined from the desorption branch of the isotherm through the Broekhoff-de Boer (BdB) method (28) and the BJH method (27).

The structure and morphology of mesoporous channels were investigated in detail by means of transmission electron microscopy (TEM, Jeol JEM 3010 UHR operating at 300 kV).

*In vitro* bioactivity assessment involved the soaking of MBG membranes in 30 ml of acellular simulated body fluid (SBF) prepared according to the protocol proposed by Kokubo and co-workers (29). The different time frames chosen for the analysis were 8, 24, 48 h and 7 days, in order to evaluate the formation of HA on samples surface also during the first hours of immersion. The solution was replaced twice a week to simulate fluid circulation in the human body; pH variations were daily monitored.

#### *Drug uptake and release*

The drug loading/release ability of the MBGs was tested by using ibuprofen, that has been used as a model drug in previous works (7-10). The absorption of ibuprofen (99.9% purity,



Sigma-Aldrich) was carried out by putting into contact a solution (9 ml) of ibuprofen in pentane ( $33 \text{ mg}\cdot\text{ml}^{-1}$ , 0.16 M) with MBG powders for 24 h under continuous stirring. The drug uptake ability was evaluated by UV-visible spectrophotometry (Cary 500 Scan UV-vis spectrophotometer); specifically, the amount of ibuprofen absorbed by the sample was calculated from the difference in the concentration of drug in solution before and after contact with the sample, on the basis of the absorption at 263 nm, typical for ibuprofen molecules. Before analysis, the samples were centrifuged to avoid scattering effect due to MBG powders suspended in the solution. The test conditions were properly set in order to allow the application of Lambert-Beer's law. A calibration curve was empirically derived by using solutions of ibuprofen in pentane of known concentrations.

The drug release kinetics were evaluated *in vitro* by soaking the MBG powders in 30 ml of stirred SBF maintained at 37 °C. At different time frames – from 1 h up to 72 h after experiment beginning – a small amount of SBF (1 ml) was picked-up and analyzed through UV-visible spectrophotometry to assess the molecule concentration in the solution. A calibration curve was calculated by using solutions of ibuprofen in SBF of known concentrations, as well as we made for uptake tests. Before spectrophotometric analysis the samples were centrifuged for eliminating possible scattering errors due to the presence of residual glass powders in the analyzed solution.

### *Biological tests*

MBG ground in powders was used for cells biocompatibility assay. The cells were not seeded directly on the material but a transwell-based method was adopted (30). Viability of cells was quantified by evaluating their mitochondrial activity; possible effects of dose-dependence were also investigated by using different amounts of MBG powders (0.5, 1.0, 1.5, 2.0 and 3.0 mg). The incubation time was set at 24 h for all the tests.

Human osteosarcoma cell line SAOS-2, obtained from the American Type Culture Collection (HTB85; ATCC), was used for the test. The cells were cultured in McCoy's 5A modified medium with 1.5 mM L-glutamine and 25 mM HEPES (Cambrex Bio Science, Baltimore, MD), supplemented with 15% foetal bovine serum, 1 mM sodium pyruvate, 100 IU/ml penicillin, 100 mg/ml streptomycin,  $10^{-8}$  M dexamethasone and 10 mM  $\beta$ -glycerophosphate (Sigma-Aldrich, Milwaukee, WI); 2.84 mM ascorbic acid, another osteogenic supplement, was present as a component of McCoy's 5A modified medium. The cells were cultured at 37 °C with 5% CO<sub>2</sub>, routinely trypsinized after reaching confluence conditions, counted and finally seeded onto the culture wells.

MBG powders were sterilized by autoclave treatment (120 °C for 20 min at 1 atm) before cytotoxicity test. The materials were applied to the base of the transwells (6.5 mm in diameter, pores size of 0.4  $\mu$ m) (Costar Transwell-Clear, Corning Costa, Cambridge, MA). To compare the relative toxicities of different materials, the transwells were transferred into 24-well culture plates that were seeded with cells ( $2.5 \times 10^5$  cells/well) for 24 h before the respective powders were transferred to the transwells. The control group (CTRL) was represented by the cases in which powders were not transferred to the culture wells. The tests were performed on triplicate samples.

To evaluate the mitochondrial activity of the seeded cells, *i.e.* the viability of SAOS-2 cells during the culture period, a test with 3-(4,5-dimethylthiazole-2-yl)-2,5-diphenyl tetrazolium bromide (MTT) (Sigma-Aldrich) was performed after incubation for 24 h. The culture medium was replaced by a 0.5 mg/ml solution of MTT in phosphate-buffered saline (PBS) (137 mM NaCl, 2.7 mM KCl, 4.3 mM Na<sub>2</sub>HPO<sub>4</sub>, 1.4 mM KH<sub>2</sub>PO<sub>4</sub>, pH = 7.4) and the cells cultures were incubated for 4 h. The test is based on the fact that viable cells can reduce MTT into formazan crystals: when reduced in a cell, either enzymatically or through direct reaction with NADH/NADPH, MTT turns to bright blue and forms a water-insoluble precipitate (formazan). After removing the MTT solution, 500  $\mu$ l of dimethyl sulphoxide

(Sigma-Aldrich) were added to solubilize the formazan products and the well plate containing the cells was shaken for 20 min on a shaker. Aliquots of 200  $\mu$ l were sampled and the related absorbance values were measured at 570 nm by a microplate reader (BioRad Laboratories, Hercules, CA). A standard curve of cell viability was used to express the results as percentage out of the total number of cells.

## RESULTS AND DISCUSSION

Examples of as-synthesized MBG membranes are reported in Figures 2a,b. After the extraction from the mould, the transparent membranes, characterized by thickness ranging within 300-500  $\mu$ m, can be easily cut in various shapes, and, for instance, disk-shaped (Figure 2a) or plug-shaped (Figure 2b) samples can be produced. The EDS spectrum of non-calcined membrane is reported in Figure 2c. It is possible to observe the peaks of silicon (Si), phosphorus (P) and calcium (Ca) due to glass oxides featuring material composition. In addition, an intense peak of carbon (C) is visible because the organic surfactant is still present inside the mesopores. The weak peak corresponding to chlorine (Cl) is due to  $\text{Cl}^-$  ions, provided by HCl entrapped in the glass structure. The presence of the silver (Ag) peak in the EDS pattern is due to the metal coating necessary for analysis. Examples of MBG membranes obtained after calcination are shown in Figures 3a,b. During calcination, the surfactant (P123) burns-out and the consolidation of the mesostructure is promoted: as known, in this phase the pores walls become thicker and the pores size decreases. The resulting calcined samples are brittle, semitransparent membranes of  $\text{SiO}_2$ - $\text{P}_2\text{O}_5$ -CaO glass, that maintain their original shape imparted before calcination. As foreseen, the calcined MBG membranes are thinner (thickness ranging within 100-300  $\mu$ m) than the as-synthesized ones; the thickness reduction is due to the shrinkage that occurs during calcination. A very weak peak of carbon (C) is distinguishable

in the EDS pattern (Figure 3c), which demonstrates that the organic surfactant was almost totally removed. Thermogravimetical analyses (Mettler Toledo TGA/SDTA 851, range of analysis 25-1000 °C, heating rate 20 °C·min<sup>-1</sup>; software: STARE 6.10) were also performed (data not reported) to quantitatively assess the residue of surfactant and, therefore, to estimate the effectiveness of calcination. Specifically, the residual organic fraction that remained entrapped inside the pores was estimated to be <5 %wt. of the initial weight of the sample.

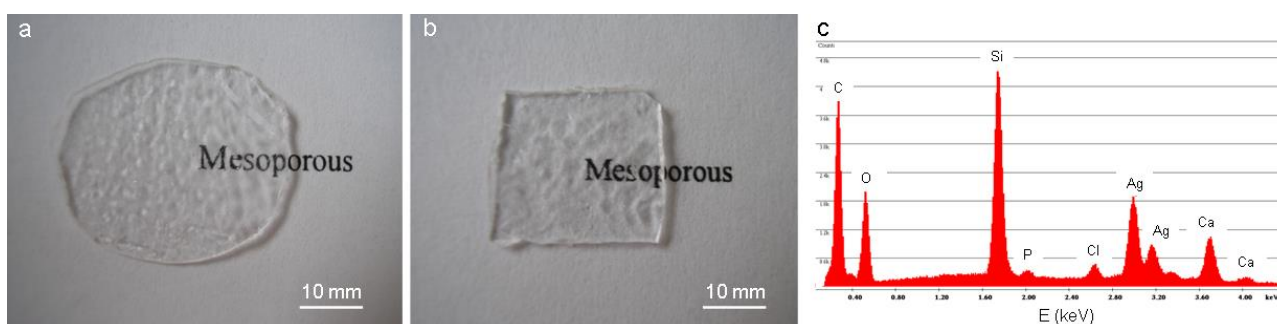


**Fig. 2** - As-synthesized mesoporous membranes: (a) disk-shaped and (b) rectangle-shaped ("plug") samples; (c) EDS pattern.

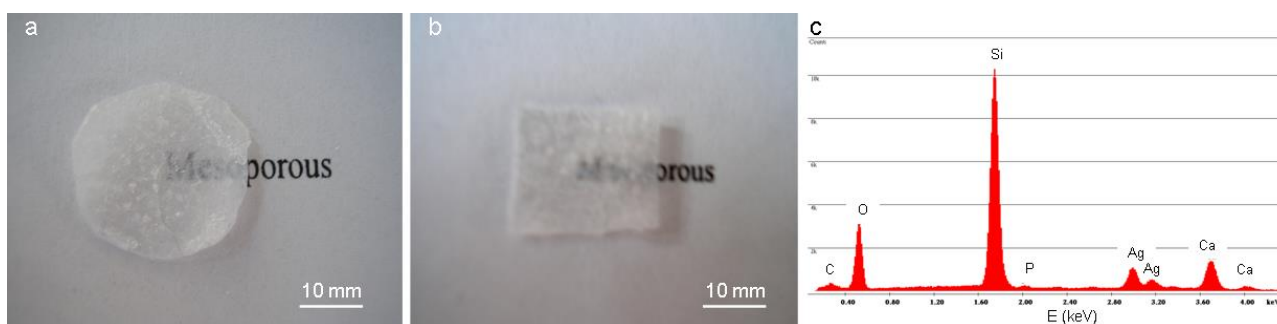


**Fig. 3** - Calcined mesoporous membranes: (a) disk-shaped and (b) rectangle-shaped ("plug") samples; (c) EDS pattern.

It is worth to notice that the final thickness of the membranes can be easily tailored: in fact, the more the sol volume cast into the mould, the higher is the thickness of the resulting

MBG membrane. The linear shrinkage, roughly calculated on the basis of membranes thickness before and after calcination, ranged within 30-40%; this important point, related to MBG membranes design and tailoring, will be further discussed at the end of the following subsection.

### *Structural analysis*

The wide-angle XRD pattern of calcined MBG is depicted in Figure 4. The presence of a broad halo between  $2\theta \approx 15.0^\circ$  and  $2\theta \approx 35.0^\circ$  demonstrates that the material is completely amorphous.

Figure 5 collects low-angle XRD investigations on the MBG before and after calcination. The spectrum of as-synthesized MBG (Figure 5a) shows a unique weak peak at  $2\theta \approx 0.93^\circ$ . The presence of this peak demonstrates that an ordered structure of mesopores already existed in the non-calcined material, but the peak intensity was weak as the surfactant (P123) filled the on-forming mesopores. After calcination, when the SDA is removed, the basal peak due to the mesophase order is clearly distinguishable at  $2\theta \approx 1.35^\circ$  (Figure 5b), together with a broad scattering at higher angles ( $2\theta \approx 1.70^\circ$ ).

The mesophase symmetry is a crucial point and was determined combining low-angle XRD results with TEM data that will be presented in the following subsection. The structure of the prepared MBG was interpreted as a 2-D hexagonal symmetry, together with some disordered wormlike domains.

By comparing the patterns shown in Figure 5, it can be observed that the position of the basal peak shifts towards a higher  $2\theta$ -value after calcination. This is due to the shrinkage of the material during calcination, *i.e.* the surfactant burning-out, which yields a decrease of the interplanar distance.

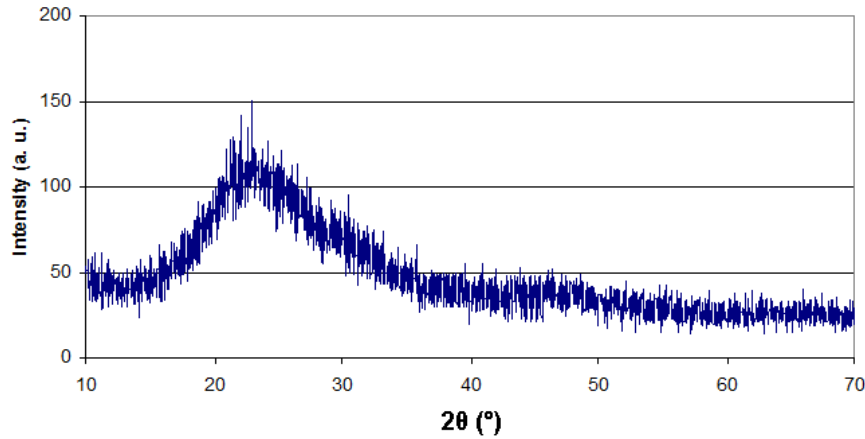


**Fig. 4** - Wide-angle XRD pattern of the calcined MBG sample.

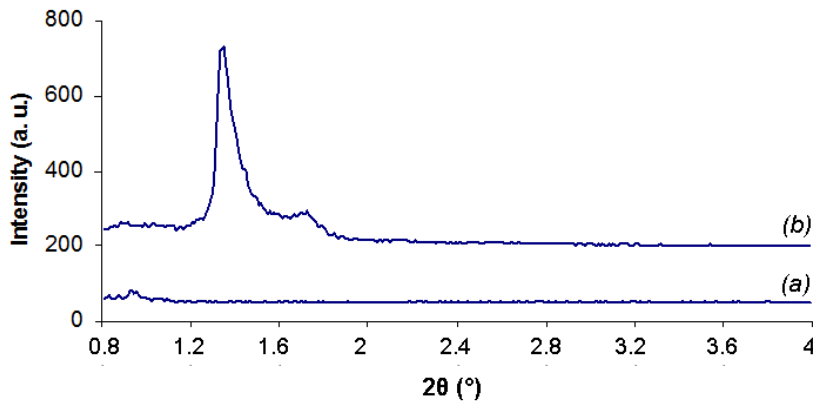


**Fig. 5** - Low-angle XRD spectra of the prepared MBG: (a) as-synthesized and (b) calcined sample.

From XRD data it is also possible to give an evaluation – although rather rough – of the shrinkage due to calcination, which should be carefully taken into account for MBG membrane design and tailoring. Assuming the basal peak being the (1 0 0) reflection of the 2-D hexagonal phase, then  $d_{100}^* = 9.40$  nm and  $d_{100} = 6.50$  nm are the interplanar distance of the non-calcined and calcined material, respectively. Hence, the cell parameters of the

mesophase before and after calcination are, respectively,  $a^* = \frac{2}{\sqrt{3}} d_{100}^* = 10.85$  nm and

$a = \frac{2}{\sqrt{3}} d_{100} = 7.50$  nm. Eventually, the linear shrinkage  $S_{lin}(\%)$  can be calculated as

$S_{lin} = \left(1 - \frac{a}{a^*}\right) \cdot 100 = 29.1$  %; this value is consistent with the range assessed qualitatively

by comparing the thickness of the MBG membranes before and after calcination. Under the assumption that the cell parameter is the characteristic dimension of the mesophase, a rough evaluation of the volumetric shrinkage  $S_{vol}(\%)$  can be finally obtained as

$$S_{vol} = \left(1 - \frac{a^3}{(a^*)^3}\right) \cdot 100 = 66.9 \text{ \%}.$$

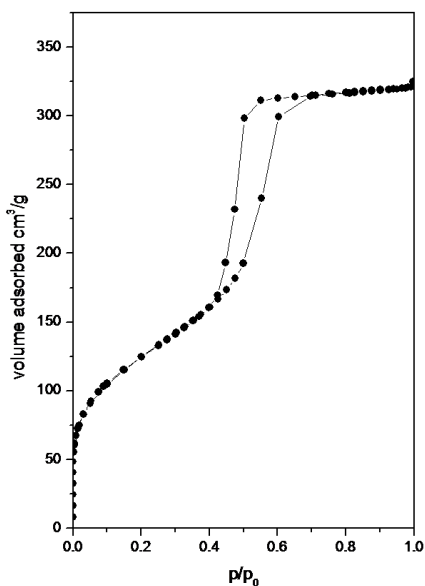
Knowing the shrinkage, the size of the mould and the volume of sol cast into the mould, it is possible – at least ideally – to design the shape and thickness of the final calcined MBG membrane, so that it can match the size and shape of patient's bone defect.

### *Mesopores characterization*

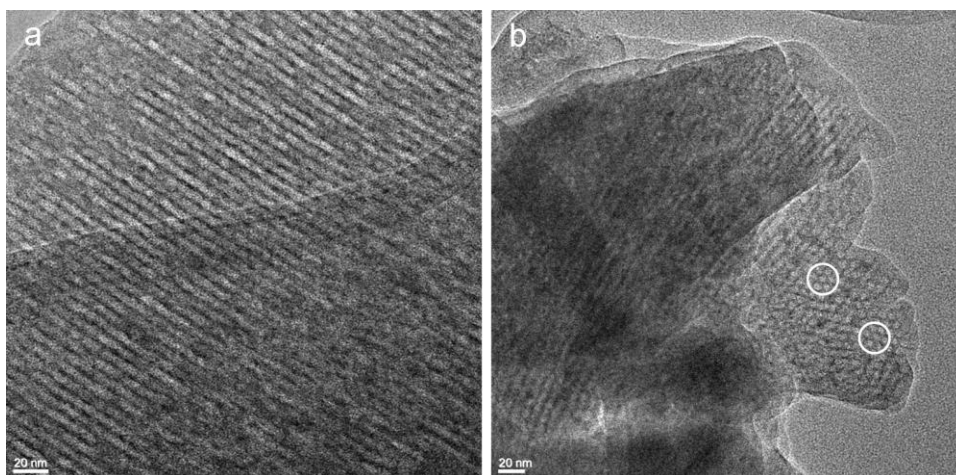
Figure 6 shows a typical IV type well-defined  $N_2$  sorption isotherm for calcined MBG ground in powders. The three relevant regions of the adsorption branch, typically corresponding to (i) monolayer/multilayer adsorption onto the mesopores surface, (ii) capillary condensation and (iii) multilayer adsorption onto the particles external surface, are clearly distinguishable. As described elsewhere, the shape of the hysteresis loop is tightly related to the shape of mesopores (31): in the present case, the MBG channels have a well defined cylindrical shape with a diameter of  $\sim 5.0$  nm (BdB and BJH methods led to very close results, as reported in Table I).

Figure 7a depicts a section along the direction parallel to channels axes, that reveals a highly ordered arrangements of 1-D open, cylindrical and parallel mesopores, as

previously inferred from  $N_2$  adsorption-desorption analysis. In Figure 7b the system of ordered parallel channels can be simultaneously seen both along the channels axes and orthogonally to them; the 2-D hexagonal symmetry of the ordered mesopores system is clearly distinguishable.



**Fig. 6** -  $N_2$  sorption isotherm of the MBGs calcined at 700 °C for 5 h.



**Fig. 7** - TEM images of the calcined MBGs. The hexagonal symmetry of the mesophase is emphasized, as an example, in two white circles.



**Table I.** TEXTURAL PARAMETERS OF THE MBG ASSESSED BY N<sub>2</sub> ADSORPTION-DESORPTION MEASUREMENTS AND TEM ANALYSIS.

Parameter	Analysis	Average value
SSA [m <sup>2</sup> ·g <sup>-1</sup> ]	BET	450.0
Pores size [nm]	BdB/BJH	5.0
	TEM	4.9
Pores wall thickness [nm]	TEM	3.0

The pores size calculated by means of N<sub>2</sub> adsorption-desorption measurements is in good accordance with that assessed by TEM, as shown in Table I. In addition, the cell parameter calculated from TEM data (7.90 nm) is consistent with that determined by XRD analysis (7.50 nm).

It should be noticed that the investigated MBG is not completely organized in ordered domains, but two different domains can be distinguished: (i) well-ordered regions according to a hexagonal symmetry and (ii) poorly ordered or disordered regions (wormlike domains).

The importance of a structure constituted by totally or partially ordered channels of nanometrical size is relevant in a material to enhance its bioactivity. As previously discussed, the mesopores texture allows to increase the surface area (Table I) available for ion-exchange phenomena, thereby promoting the bioactivity process and the kinetics of HA formation.

#### *In vitro bioactivity tests*

Figure 8 collects the SEM micrographs of MBG membrane surface after soaking for 8, 24, 48 h and 7 days in SBF; the corresponding EDS spectra are also reported. After 8 h of immersion, globe-shaped agglomerates are already distinguishable on the MBG membrane (Figure 8a). The newly formed phase, whose formation is due to ion-exchange phenomena between the MBG and the solution, is apatite-like, as qualitatively assessed by the EDS spectrum reported in Figure 8b. An intense peak corresponding to silicon (Si) is clearly visible in the pattern and can be attributed to (i) the presence of a silica-gel layer, according to the bioactivity process proposed by Hench and co-workers (32,33) and/or (ii) a substrate effect due to the finite volume of EDS analysis ( $\sim 1 \mu\text{m}^3$ ). The Si-peak becomes progressively weaker as the soaking time increases (Figures 8d and 8f) and it is no more visible after 7 days of soaking (Figure 8h). This demonstrates that the newly formed phase progressively grew in amount and thickness, and finally the typical “cauliflower” morphology of HA can be recognized after soaking for 7 days (Figure 8g)

The quantitative EDS data reported in Table II show that the agglomerates visible on the membrane after 8 h of soaking in SBF can be identified as Ca-deficient HA ( $\text{Ca/P} = 1.51$ ). The Ca content in the newly formed phase progressively rises as the soaking time increases; after 7 days, a molar Ca/P ratio of 1.67, corresponding to the stoichiometric Ca/P ratio of natural HA, was detected.

The XRD pattern reported in Figure 9 shows, as expected, several marked peaks assignable to the (0 0 2), (2 1 1), (3 0 0), (2 0 2) and (2 1 3) reflections of HA. The main (double) peak at  $2\theta \approx 32.0^\circ$  is broad due to the microcrystalline nature of the HA nucleated on MBG surface.

It is worth to underline that the prepared MBG membranes, although having a silica content of 80% mol., are highly bioactive. Hench and co-workers demonstrated that, for traditional melt-derived glasses, the silica content has to be 60 %mol. or less to allow to bond with bone (34). Nevertheless, bone bonding can be achieved for sol-gel glasses with

up to 90 %mol. of  $\text{SiO}_2$ , due to their high surface area, typically within  $100\text{-}200\text{ m}^2\cdot\text{g}^{-1}$  (about two order of magnitude higher than that of melt-derived glasses) (35,36).

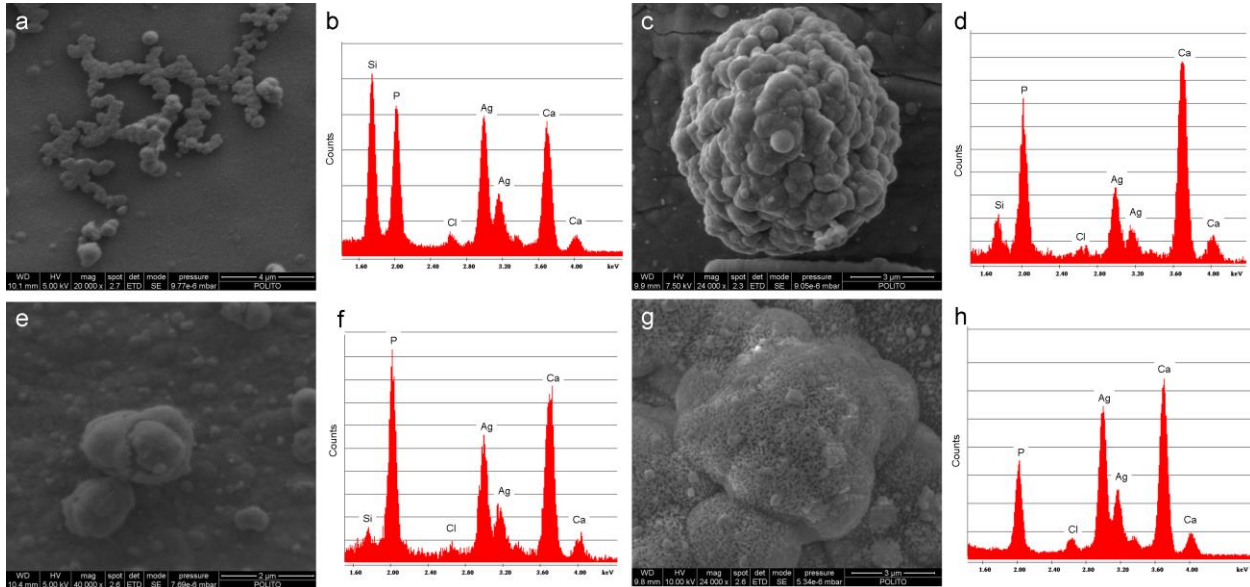


**Fig. 8** - Surface micrographs and corresponding compositional analyses of the MBG membranes after soaking in SBF for (a,b) 8 h; (c,d) 24 h; (e,f) 48 h; (g,h) 7 days.

**Table II.** EDS ANALYSIS (SEMIQUANTITATIVE EVALUATION) ON THE SURFACE OF THE MBG MEMBRANES SOAKED IN SBF.

Soaking time	Ca/P (molar ratio)
8 h	1.51
24 h	1.58
48 h	1.62
7 days	1.67

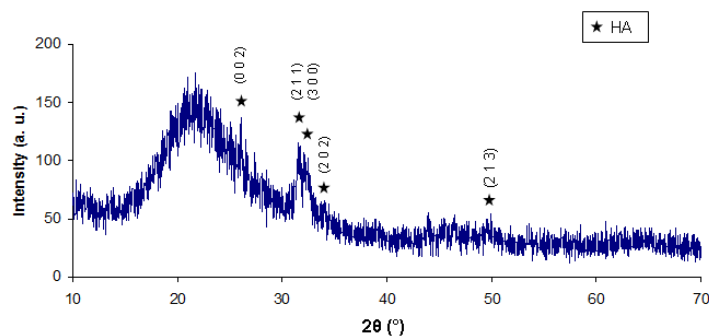


**Fig. 9** - XRD pattern of the MBGs after soaking for 7 days in SBF.

The excellent bioactive properties observed for the prepared MBG membranes can be explained considering that the nanoporous texture of the material plays a key role in enhancing its surface area. In fact, the system of mesoporous channels enhances the surface area up to values still higher (Table I) than those exhibited by sol-gel glasses. Therefore, the ion-exchange phenomena between MBG and SBF *in vitro* or between MBG and the biological fluids *in vivo* can be remarkably promoted. The presence of an ordered mesostructure significantly affects the bioactive properties of the glass and, generally, has more influence than glass chemical composition in the HA nucleation stage during the bioactivity process (23).

The pH variation in the solution, resulting from ion-exchanges with the material, is quite moderate (pH < 8.0; reference value for SBF = 7.40), thus no cytotoxic effect induced by the material, when implanted, is foreseen.

#### *Drug uptake and release ability*

The potential of mesoporous materials of acting as matrices for the encapsulation and subsequent release of drug molecules has been underlined in many research works, as the size of the mesopores can be designed to match, at least approximately, the sizes of a

wide range of biomolecules. Since the material synthesized in this work exhibited a very high bioactivity with fast kinetics of HA formation, it was very interesting to assess if such a property could negatively affect the drug release ability of the MBG. In fact, one might reasonably hypothesize that the HA agglomerates, formed during immersion in SBF, can obstruct the mesoporous channels, thereby inhibiting – or strongly depressing – the ibuprofen release from the material.

The test of ibuprofen uptake was carried out in duplicate to have a control of the test repeatability. Actually, the test was found to be highly repeatable, as the analyses on both samples led to analogous results. It was estimated that the material could absorb an ibuprofen amount equal to ~25 %wt. of its starting weight. This value is slightly higher than that obtained by Izquierdo-Barba *et al.* (37) who tested mesoporous materials belonging to the SBA-15 family characterized by mesopores size similar to that of the MBGs prepared in this work. The amount of ibuprofen absorbed by MBG powders was also found comparable to the data obtained testing mesophases with smaller pores, *e.g.* MCM-41 (8-10), that should be expected to exhibit a higher affinity for ibuprofen molecules due to a better dimensional matching between drug molecule length and pore size.

According to the uptake tests, also the ibuprofen release tests were performed in duplicate, and both of them led to similar results. Figure 10 shows the kinetics of ibuprofen delivery in SBF. Above 90% of the drug absorbed into the mesopores was released within the first two hours of soaking and, therefore, before HA formation occurred. Hence, HA growth and ibuprofen release followed quite separate kinetics and, specifically, the material bioactivity does not negatively interfere with the drug release ability of MBG. After the first 24 h of analysis, the percentage of released ibuprofen seems to decrease progressively (from 96% after 24 h up to 93% after 50 h); this phenomenon may be explained considering that the material, after releasing most of the absorbed drug, can re-uptake a small amount of it. The release kinetics from the MBG are very similar to those

obtained by Izquierdo-Barba *et al.* testing SBA-15 spheres (37), that have mesopores size comparable to that of the prepared MBGs.

### *Biological compatibility and cytotoxicity*

The mitochondrial activity of SAOS-2 cells was used as a reliable index for quantifying their viability. Figure 11 reports the results after cells incubation for 24 h in response to different MBG amounts. Control sample (CTRL; medium only without MBG powders) exhibits a cells viability of ~90% (< 100%); this occurs because a cells fraction (~10% in the present case) is damaged by the intrinsic oxidative stress due to cells manipulation during test procedures.

In comparison with CTRL, the presence of MBG powders did not seem to significantly affect cells viability, that remain very high (>75%) in all the experiments. Cells viability did not seem to be compromised by the presence of MBG; further tests for investigating the material effect after time frames longer than 24 h are currently in progress. From the data reported in Figure 11, a high MBG amount seems to emphasize cells viability (maximum viability was registered in presence of 3 g of MBG); however, it is not surprising as it is known that bioactive glasses can influence the cycle, metabolism and activity of cells (38). It should be considered that MBGs are highly reactive and, specifically, Si and Ca ions released from the glass can exert a gene control regulation emphasizing the activity of bone cells (39-41).

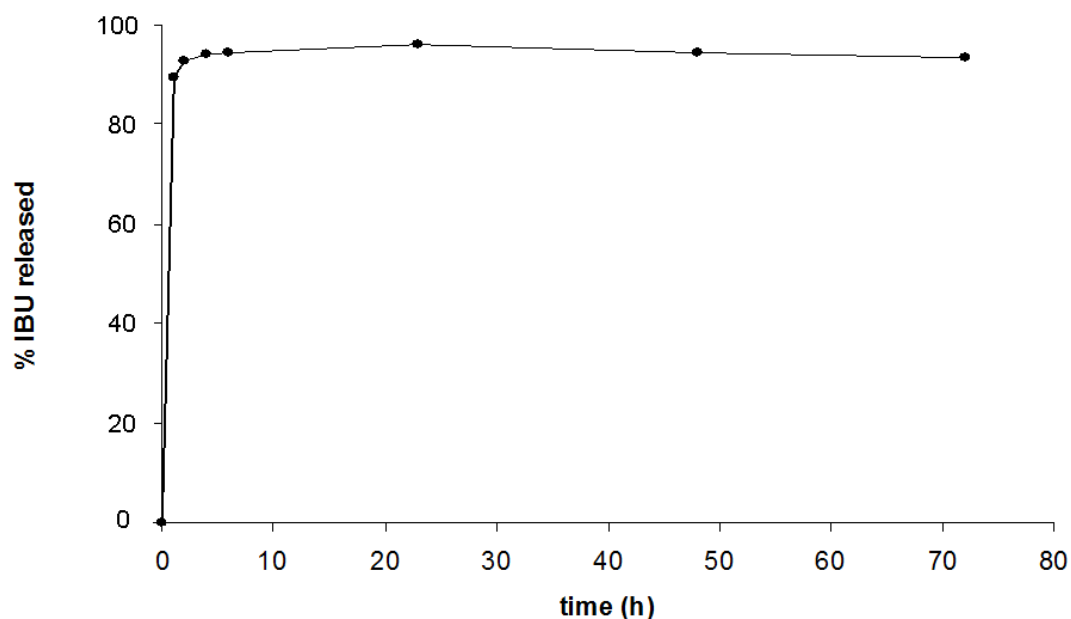


**Fig. 10** - *Ibuprofen release kinetics from MBG powders in SBF.*

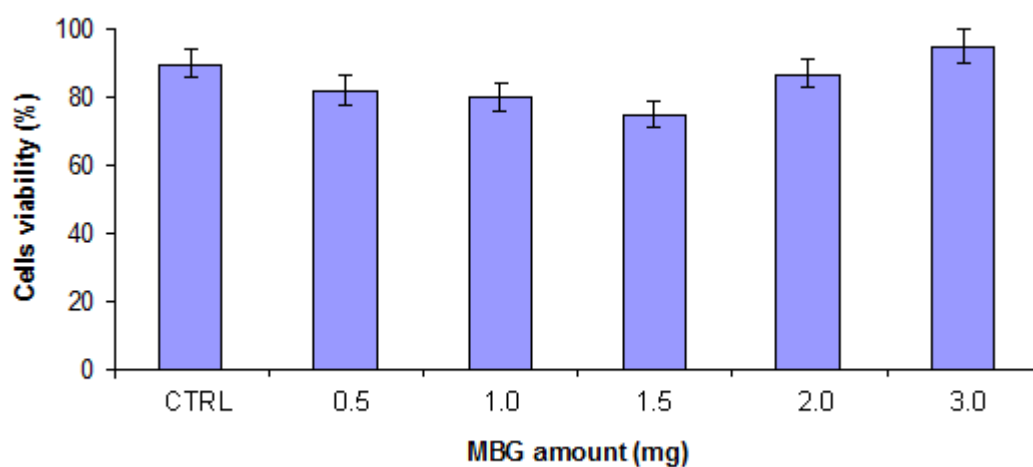


**Fig. 11** - *Viability of SAOS-2 cells after incubation for 24 h in presence of MBG powder by using the transwell culture method.*

## CONCLUSIONS

Mesoporous glass belonging to the  $\text{SiO}_2\text{-CaO-P}_2\text{O}_5$  ternary system was successfully synthesized in form of membranes with adjustable thickness in the 100-300  $\mu\text{m}$  range.

After calcination, the glass exhibited an ordered structures of mesopores (pores size ~5 nm) ascribable to hexagonal symmetry. The presence of an ordered texture of mesopores eventually resulted in excellent bioactive properties, as the pores contributed remarkably in increasing the specific surface area of the material ( $\sim 450 \text{ m}^2 \cdot \text{g}^{-1}$ ), thereby enhancing the ion-exchange phenomena between glass and solution during immersion in SBF. This led to the fast formation (within 8 h) of a calcium-phosphate layer on the membrane surface; such a newly formed phase progressively crystallizes in HA, characterized by its typical globular “cauliflower” morphology. In addition, the mesoporous structure imparted to the material the ability of encapsulating ibuprofen molecules within its mesochannels. Ibuprofen release from MBG in SBF occurred with kinetics similar to that observed for pure silica mesophases with analogous pores size. Finally, the MBG exhibited an excellent cells tolerance, without negatively affecting SAOS-2 cells viability during *in vitro* tests.

As a whole, the results suggest the potential use of the prepared MBG in bone tissue engineering as a bioactive drug release system suitable for bone defect fillers and controlled local drug therapy.

## REFERENCES

1. Haber J. Manual on catalyst characterization. Pure Appl Chem 1991; 63: 1227-46.
2. Grun M, Unger KK, Matsumoto A, Tsutsumi K. Novel pathways for the preparation of mesoporous MCM-41 materials: control of porosity and morphology. Microp Mesop Mater 1999; 27: 207-16.
3. Soler-Illia GJDA, Crepaldi EL, Grosso D, Sanchez C. Block copolymer-templated mesoporous oxides Curr Opin Colloid Interface Sci 2003; 8: 109-26.



4. Kresge CT, Leonowicz ME, Roth WJ, Vartuli JC, Beck JS. Ordered mesoporous molecular sieves synthesized by a liquid-crystal template mechanism. *Nature* 1992; 359: 710-2.
5. Zhao D, Huo Q, Feng J, Chmelka BF, Stucky DJ. Nonionic triblock and star diblock copolymer and oligomeric surfactant syntheses of highly ordered, hydrothermally stable, mesoporous silica structures. *J Am Chem Soc* 1998; 120: 6024-36.
6. Vallet-Regí M, Ramila A, Del Real R, Perez-Pariente J. A new property of MCM-41: drug delivery system. *Chem Mater* 2001; 13: 308-11.
7. Cauda V et al. SBA-15 ordered mesoporous silica inside a bioactive glass-ceramic scaffold for local drug delivery. *J Mater Sci: Mater Med* 2008; 19: 3303-10.
8. Mortera R et al. Synthesis of MCM-41 spheres inside bioactive glass-ceramic scaffold. *Chem Eng J* 2008; 137: 54-61.
9. Vitale-Brovarone C, Baino F, Miola M, Mortera R, Onida B and Verné E. Glass-ceramic scaffolds containing silica mesophases for bone grafting and drug delivery. *J Mater Sci: Mater Med* 2009; 20: 809-20.
10. Mortera R et al. Monodisperse mesoporous silica spheres inside a bioactive macroporous glass-ceramic scaffold. *Adv Eng Mater* 2010; 12: 256-9.
11. Vallet-Regi M, Izquierdo-Barba I, Ramila A, Perez-Pariente J, Babonneau F, Gonzalez-Calbet J. Phosphorous-doped MCM-41 as bioactive material. *Solid State Sci* 2005; 7: 233-7.
12. Horcajada P, Ramila A, Boulahya K, Gonzalez-Calbet J, Vallet-Regi M. Bioactivity in ordered mesoporous materials. *Solid State Sci* 2004; 6: 1295-300.
13. Ozawa N, Negami S, Odaka T, Morii T, Koshino T. Histological observations on tissue reaction of the rat calcaneal tendon to sintered hydroxyapatite. *J Mater Sci Lett* 1989; 8: 869-71.

14. Dorozhkin SV. Bioceramics of calcium orthophosphates. *Biomaterials* 2010; 31: 1465-85.
15. Hench LL. Bioactive materials: the potential for tissue regeneration. *J Biomed Mater Res* 1998; 41: 511-8.
16. Jones JR, Ehrenfried LM, Hench LL. Optimising bioactive glass scaffolds for bone tissue engineering. *Biomaterials* 2006; 27: 964-73.
17. Hench LL, Splinter RJ, Allen WC, Greenlee TK. Bonding mechanisms at the interface of ceramic prosthetic materials. *J Biomed Mater Res* 1972; 5: 117-41.
18. Vallet-Regi M, Ragel CV, Salinas AJ. Glasses with medical application. *Eur J Inorg Chem* 1993; 6: 1029-42.
19. Pereira MM, Clark AE and Hench LL. Calcium phosphate formation on sol-gel-derived bioactive glasses in vitro. *J Biomed Mater Res* 1994; 28: 693-8.
20. Hench LL. Sol-gel materials for bioceramics applications. *Curr Opin Solid State Mater Sci* 1997; 2: 604-10.
21. Xia W, Chang J. Well ordered mesoporous bioactive glasses (MBG): a promising bioactive drug delivery system. *J Control Rel* 2006; 110: 522-30.
22. Xia W, Chang J. Preparation, in vitro bioactivity and drug release property of well ordered 58S bioactive glass . *J Non-Cryst Solids* 2008; 354: 1338-41.
23. Lopez-Noriega A, Arcos D, Izquiendo-Barba I, Sakamoto Y, Terasaki O, Vallet-Regi M. Ordered mesoporous bioactive glasses for bone tissue regeneration. *Chem Mater* 2006; 18: 3137-44.
24. Shi QH, Wang JF, Zhang JP, Fan J, Stucky GD. Rapid-setting, mesoporous, bioactive glass cements that induce accelerated in vitro apatite formation. *Adv Mater* 2006; 18: 1038-42.
25. Brinker CJ, Lu YF, Sellinger A, Fan HY. Evaporation-induced self-assembly: nanostructures made easy. *Adv Mater* 1999; 11: 579-85.

26. Yan X, Yu C, Zhou X, Tang J, Zhao D. Highly ordered mesoporus bioactive glasses with superior in vitro bone-forming bioactivities. *Angew Chem Int Ed* 2004; 43: 5980-4.
27. Brunauer S, Emmet PH, Teller E. Adsorption of gases in multimolecular layers. *J Am Chem Soc* 1938; 60: 309-19.
28. Broekhoff JCP, De Boer JH. Studies on pore systems in catalysts: IX. Calculation of pore distributions from the adsorption branch of nitrogen sorption isotherms in the case of open cylindrical pores A. Fundamental equations. *J Catal* 1967; 9: 8-14.
29. Kokubo T, Takadama H. How useful is SBF in predicting in vivo bone bioactivity? *Biomaterials* 2006; 27: 2907-15.
30. Kuo TC, Lee BS, Kang SH, Lin FH, Lin CP. Cytotoxicity of DP-Bioglass paste used for the treatment of dentin hypersensitivity. *J Endod* 2007; 33: 451-4.
31. Satterfield CN. Heterogeneous catalysis in industrial practice. New York: Mc Graw-Hill 1991.
32. Wilson J, Pigott GH, Schoen FJ, Hench LL. Toxicology and biocompatibility of bioglasses. *J Biomed Mater Res* 1981; 15: 805-17.
33. Cao W, Hench LL. Bioactive materials. *Ceram Int* 1996; 22: 493-507.
34. Hench LL, Wilson J. An introduction to bioceramics. Singapore: World Scientific 1993.
35. Sepulveda P, Jones JR, Hench LL. In vitro dissolution of melt-derived 45S5 and sol-gel derived 58S bioactive glasses. *J Biomed Mater Res* 2002; 61: 301-11.
36. Pereira MM, Jones JR, Hench LL. Bioactive glass and hybrid scaffolds prepared by sol-gel method for bone tissue engineering. *Adv Appl Ceram* 2005; 104: 35-42.
37. Izquierdo-Barba I et al. Influence of mesoporous structure type on the controller delivery of drugs: release of ibuprofen from MCM-48, SBA-15 and functionalized SBA-15. *J Sol-Gel Sci Technol* 2009; 50: 421-9.

38. Hench LL. Genetic design of bioactive glasses. *J Eur Ceram Soc* 2008; 29: 1257-65.
39. Xynos ID, Hukkanen MV, Batten JJ, Buttery LD, Hench LL, Polak JM. Bioglass 45S5 stimulates osteoblast turnover and enhances bone formation In vitro: implications and applications for bone tissue engineering. *Calcif Tissue Int* 2000; 67: 321-9.
40. Xynos ID, Edgar AJ, Buttery LD, Hench LL, Polak JM. Gene-expression profiling of human osteoblasts following treatment with the ionic products of Bioglass 45S5 dissolution. *J Biomed Mater Res* 2001; 55: 151-7.
41. Hench LL, Xynos ID, Polak JM. Bioactive glasses for in situ tissue regeneration. *J Biomater Sci Polym Ed* 2004; 15: 543-62.

## Figure legends

**Fig. 1.** Flow-chart of the procedure followed for manufacturing the mesoporous glass.

**Fig. 2.** As-synthesized mesoporous membranes: (a) disk-shaped and (b) rectangle-shaped (“plug”) samples; (c) EDS pattern.

**Fig. 3.** Calcined mesoporous membranes: (a) disk-shaped and (b) rectangle-shaped (“plug”) samples; (c) EDS pattern.

**Fig. 4.** Wide-angle XRD pattern of the calcined MBG sample.

**Fig. 5.** Low-angle XRD spectra of the prepared MBG: (a) as-synthesized and (b) calcined sample.

**Fig. 6.** N<sub>2</sub> sorption isotherm of the MBGs calcined at 700 °C for 5 h.

**Fig. 7.** TEM images of the calcined MBGs. The hexagonal symmetry of the mesophase is emphasized, as an example, in two white circles.

**Fig. 8.** Surface micrographs and corresponding compositional analyses of the MBG membranes after soaking in SBF for (a,b) 8 h; (c,d) 24 h; (e,f) 48 h; (g,h) 7 days.

**Fig. 9.** XRD pattern of the MBGs after soaking for 7 days in SBF.

**Fig. 10.** Ibuprofen release kinetics from MBG powders in SBF.

**Fig. 11.** Viability of SAOS-2 cells after incubation for 24 h in presence of MBG powder by using the transwell culture method.